Blue-light-emitting color centers in high-quality hexagonal boron nitride

Brian Shevitski ⦿,[1,2,3,4] S. Matt Gilbert,[1,2,3] Christopher T. Chen,[4] Christoph Kastl,[4,5] Edward S. Barnard,[4] Ed Wong,[4]
D. Frank Ogletree,[4] Kenji Watanabe,[6] Takashi Taniguchi,[6] Alex Zettl,[1,2,3,*] and Shaul Aloni[4,†]

[1]*Department of Physics, University of California at Berkeley, Berkeley, California 94720, USA*
[2]*Materials Sciences Division, Lawrence Berkeley National Laboratory, Berkeley, California 94720, USA*
[3]*Kavli Energy NanoScience Institute at the University of California, Berkeley, and the Lawrence Berkeley National Laboratory,*
Berkeley, California 94729, USA
[4]*The Molecular Foundry, Lawrence Berkeley National Laboratory, Berkeley, California 94720, USA*
[5]*Walter-Schottky-Institute and Physik Department, Technical University of Munich, 85748 Garching, Germany*
[6]*Advanced Materials Laboratory, National Institute for Materials Science, 1-1 Namiki, Tsukuba 305-0044, Japan*

Light emitters in wide-band-gap semiconductors are of great fundamental interest and have potential as optically addressable qubits. Here we describe a unique color center in high-quality hexagonal boron nitride (h-BN) with a sharp emission line at 435 nm. The emitters are activated and deactivated by electron beam irradiation and have spectral and temporal characteristics consistent with atomic color centers weakly coupled to lattice vibrations. The emitters are conspicuously absent from commercially available h-BN and are present in only ultrahigh-quality h-BN grown using a high-pressure, high-temperature Ba-B-N flux/solvent, suggesting that these emitters originate from impurities or related defects specific to this unique synthetic route. Our results imply that the light emission is activated and deactivated by electron beam manipulation of the charge state of an impurity-defect complex.

I. INTRODUCTION

Luminescent defects in wide-band-gap semiconductors are of great importance for both fundamental physics and future technological applications. Many of these defects are single-photon emitters (SPEs), a likely component of next-generation information technologies, especially quantum cryptography [1,2] and information processing [3–5]. SPEs embedded in solid-state systems are particularly significant for widespread adoption of these emerging technologies as they offer a promising route toward scalable deployment of new integrated quantum circuits. The diamond nitrogen-vacancy (NV) center has been the leading candidate for solid-state SPE applications because it can easily be manipulated and read out at room temperature using existing optical methods [6,7]. Due to the technical difficulty of synthesizing and fabricating diamond-based devices, greater attention has been placed on finding new solid-state SPE systems [8,9] with particular emphasis placed on two-dimensional (2D) material systems, especially sp^2-bonded hexagonal boron nitride (h-BN) [10–14].

h-BN, or "white graphite," has been of great interest to the nanoscience community over the last several decades, in part because it is isostructural to graphite and forms many of the same types of nanostructures as sp^2-bonded carbon, but with different electronic and thermodynamic properties [15–19]. h-BN is especially important to the expanding study of 2D

materials because it is atomically flat, inert, and electrically insulating, making it an ideal substrate for testing new physics in low-dimensional materials [20]. Recently, it was shown that the local structure of h-BN can be controlled via electron irradiation [21,22] and synthetic methods [23], allowing for additional material control.

In this paper we report a unique color center in high-quality h-BN, activated and characterized by an electron beam. We show that these emitters are highly localized, are spectrally pure, and have an emission signature indicative of weak lattice coupling at room temperature. These properties make this color center a promising candidate for future applications in quantum information science.

II. EXPERIMENT

Ultrahigh-quality h-BN crystals used in this study (generally accepted as the best substrates available for sensitive device applications and scanning probe measurements) were synthesized using a Ba-B-N solvent precursor at high temperature and high pressure at the National Institute for Materials Science (NIMS) by Taniguchi and Watanabe [24]. We refer to this material throughout the text as NIMS-BN. Millimeter-size crystallites are mechanically exfoliated using blue wafer dicing tape and transferred onto $p + +$ silicon substrates (0.001–100 Ω cm) with a few-nanometer-thick native oxide layer. Samples of commercially available h-BN (Alfa Aesar 040608) are similarly exfoliated and transferred and then annealed at 850 °C in argon at 1 Torr for 1 h before characterization.
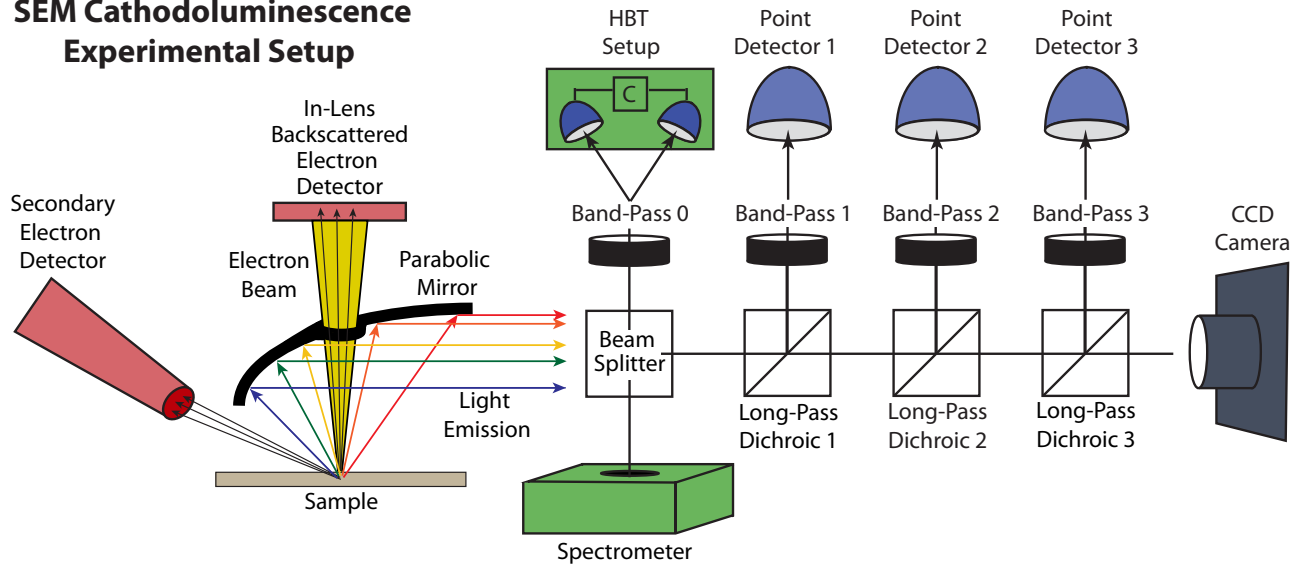
*azettl@berkeley.edu
†saloni@lbl.gov

FIG. 1. Experimental setup for measuring cathodoluminescence in the scanning electron microscope (SEM). The electron beam excites the sample and causes it to fluoresce. The resulting light is then used for hyperspectral imaging by a spectrometer (slow acquisition, low signal-to-noise ratio, high spectral resolution) and point detectors (fast acquisition, high signal-to-noise ratio, low spectral resolution). A Hanbury Brown–Twiss (HBT) apparatus is used to measure the second-order coherence function $g^2(\tau)$ of the light emission.

We use cathodoluminescence (CL) in a scanning electron microscope (SEM) to activate and characterize light emission from the h-BN. CL measurements are performed using the home-built SEM CL system shown in Fig. 1. The system is built around a Zeiss Gemini Supra 55 VP-SEM operated at accelerating voltages between 2 and 10 keV with beam currents in the 100–1500-pA range. Light emission from the sample is collected by a parabolic mirror and directed down an optical path for characterization. Synchronous data from SEM (secondary electron and in-lens detectors) and optical (photon-counting point detectors and spectrometer) channels are acquired using the Molecular Foundry SCOPEFOUNDRY software [25]. All experiments are conducted at room temperature.

As the electron beam is rastered across the sample, the light emission from each point of the scan can be coupled into an optical fiber (Thorlabs FG200UEA) using a UV-enhanced parabolic aluminum reflector and recorded using a spectrometer (Princeton Instruments SP2300i) with a CCD camera (Andor 970-UVB) to capture the spectral distribution of the light at each pixel, resulting in a three-dimensional data set we refer to as a spectral image (SI). The spectra are not intensity corrected for the wavelength-dependent efficiency of the spectrometer grating and CCD camera.

Alternatively, the light can be directed through a series of dichroic mirrors and bandpass filters to an array of photon-counting photomultiplier tube point detectors (Hamamatsu H7360-01, Hamamatsu H7421-40, and Hamamatsu H7421-50), resulting in intensity images of well-defined wavelength bands. We refer to such data throughout the text as bandpass (BP) images.

The time correlation of the emitted light can be measured by coupling to a Hanbury Brown–Twiss (HBT) setup. The arrival times of photons at the detectors in both arms of the apparatus are recorded with 50-ps resolution, and a coincidence histogram as a function of delay time between the two detectors is made. The raw coincidence histogram is then normalized by the number of coincidences at long delay times. A background correction is performed using the signal-to-background ratio estimated independently for each measurement [26], resulting in a measurement of the second-order autocorrelation function $g^2(\tau)$ of the emitted light (see the Supplemental Material for details [27]).

All data analysis is performed using common open-source packages in the PYTHON programming language. Multivariate statistical analysis of hyperspectral images is carried out using the HYPERSPY PYTHON package [28].

III. RESULTS

We first describe results from NIMS-BN. In order to activate and characterize individual emitters, we initially identify large (lateral size of 10–100 μm) flakes of h-BN using the raster scan images from the SEM electron detectors, shown in Fig. 2(a). Optical and atomic force microscopy observations of our samples indicate that the flakes generally have thicknesses of tens to hundreds of nanometers. Relevant spectral bands for BP imaging are determined by inspection of the average CL spectrum, shown in Fig. 2(b), obtained by integrating spectra while continuously scanning a single flake. We isolate the primary spectral regions of interest [indicated by the vertical lines and shaded regions in Fig. 2(b)]: 280–409 nm (UV), 430–470 nm (blue), and 485–735 nm [visible (Vis)] for BP imaging with appropriate dichroic and bandpass optics.

There are several striking features in each channel of the BP images. Figure 2(c) shows the spatial distribution of the previously reported UV emitters in the h-BN flake [14]. The emitters have a pointlike character and are densely and uniformly distributed across the entire h- BN crystal, with enhanced emission along linelike features that are likely
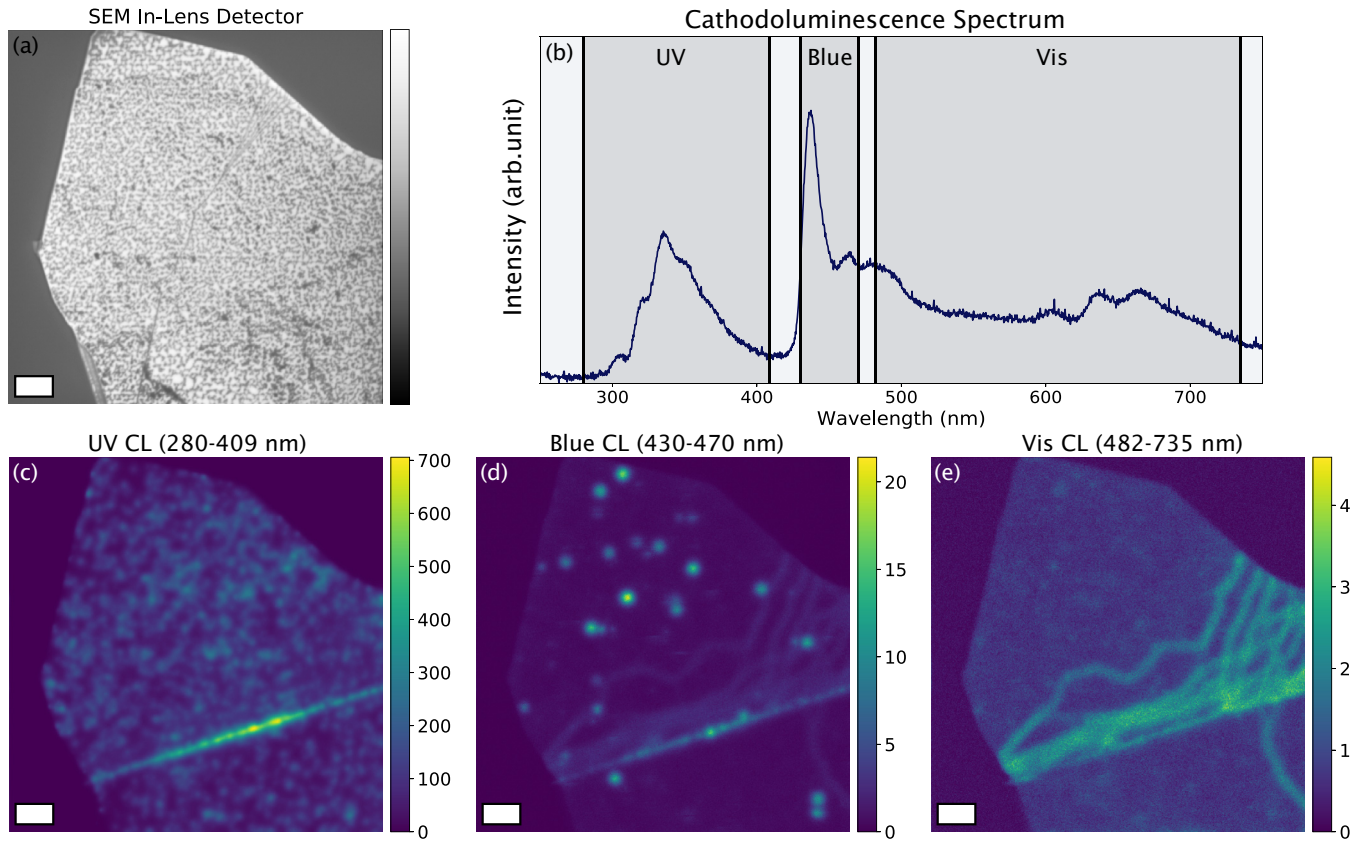
FIG. 2. Overview of light emission from h-BN. An SEM image of a flake of h-BN is shown in (a); the scale bar is 1 μm. (b) shows the mean CL response from the sample, with the three main spectral bands of interest indicated by vertical lines and shaded regions. (c)–(e) show the light emission from the flake in each of these three spectral bands (wavelength range listed above each image, intensity scale in counts/pixel). (c) shows UV light emission from a high density of pointlike emitters as well as bright emission from a large linelike feature. The intensity in the blue band arises mostly from the pointlike emitters, shown in (d). (e) shows the spatial distribution of intensity from the green to red region of the spectrum (Vis). Emission in this band arises mostly from extended defects in the crystal. The images are generated by averaging 17 consecutive scans, each with a pixel dwell time of 28.6 μs/pixel.

associated with extended line defects [29] or strain caused by a wrinkle or fold in the crystallite [30]. Figure 2(e) shows very weak extended features in the Vis band (485–735 nm), as previously reported [29]. These features are localized at grain boundaries and dislocations within the h-BN crystal. No localized, pointlike sources of light emission are observed within this band using CL BP imaging.

The bright, pointlike features in the blue BP image between 430 and 470 nm in Fig. 2(d) show the unique color centers in NIMS-BN that are the focus of this study. They appear slightly larger and less dense compared to the UV emitters in the previous panel. Also present is the linelike feature from the UV band, as well as a very weak signal from extended features in the Vis band. The broad spectral character of these extended features results in residual intensity leaking into the blue band.

We further characterize electron-stimulated light emission from NIMS-BN using hyperspectral CL imaging by collecting a CL spectrum from each pixel in a raster scan. To isolate the unique spectral signature of each type of emitter we perform a non-negative matrix factorization decomposition [31] of the spectra in the SI into four components that visualize the main features present in the data set. Figures 3(a)– 3(f) show the results of the decomposition. Each image (also called

the decomposition loading or decomposition weight) shows the relative abundance of each associated spectral component (also called the decomposition factor) below. The vertical red lines in Figs. 3(a), 3(c), and 3(e) show the passband used for BP imaging in Figs. 2(c), 2(d), and 2(e), respectively.

The first component (see the Supplemental Material [27]) is a spatially uniform background that reflects dark counts, noise, and nonlocalized light emission. The component shown in Figs. 3(e) and 3(f) shows the light emission of extended line defects, as well as a small number of highly localized features with appreciable intensity that are consistent with previous photoluminescence (PL) studies [10,11] of SPEs in h-BN. Figure 3(a) shows a dense collection of pointlike emitters, similar to the UV BP image in Fig. 2(b). The spectral features in the component in Fig. 3(b) are a close match to UV SPEs in h-BN seen in previous CL studies [14].

The most striking feature, shown in Figs. 3(c) and 3(d), closely resembles the spectral and spatial signatures of a typical color center in a wide-band-gap semiconductor [10,12]. Specifically, they are highly localized and spectrally sharp, and the first peak is followed by additional spectral features shifted by tens of meV that are interpreted as evidence of electron-phonon coupling. This component is investigated further in Fig. 3(g) using multi-Gaussian fitting of the spectral
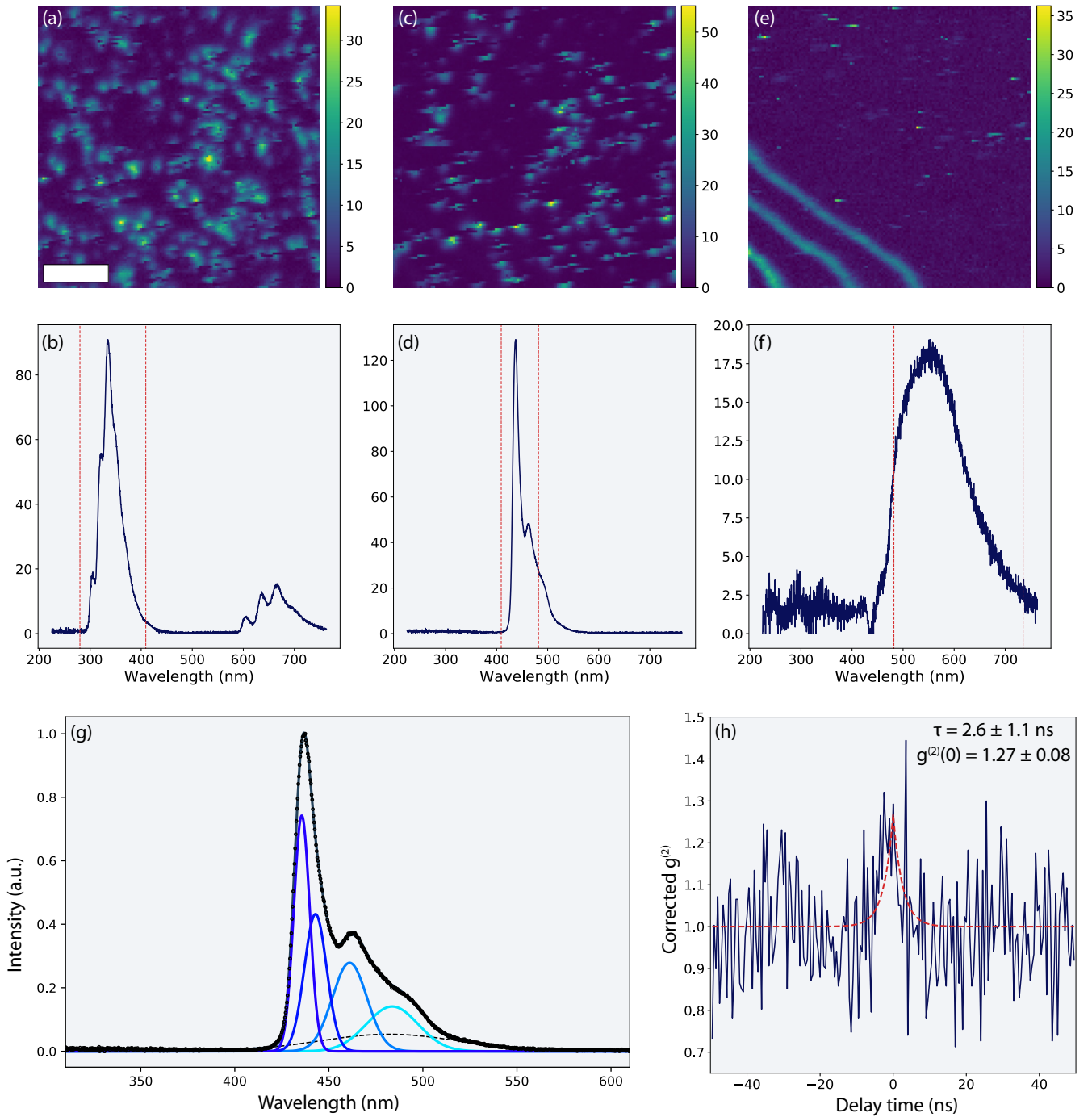
FIG. 3. Hyperspectral characterization of a dense array of emitters across three spectral regions in h-BN. Hyperspectral CL data are decomposed using non-negative matrix factorization to display the main features of the data. Each image component (top row, scale bar is 1 μm) shows the spatial distribution of the associated spectral component below (middle row). The red lines on the spectral components in (b), (d), and (f) show the edges of the bandpass filters used in bandpass imaging from Fig. 2. The (a) spatial and (b) spectral distributions of the first component show pointlike UV emitters from 300 to 400 nm. The peaks between 600 and 700 nm are artifacts due to the second-order reflections of the UV light from the spectrometer grating. (c) and (d) show the spectral signature of the blue color centers between 400 and 500 nm. (e) and (f) show extended emission features between 500 and 700 nm, likely caused by extended defects and/or strain. (g) shows a rescaled view of the blue emission component as well as the results of multi-Gaussian fitting of the peak. The fitted components show a zero-phonon line followed by several phonon replicas with decreasing amplitude, an indicator of a single-photon emitter weakly coupled to the lattice. The photon-correlation curve in (h) shows a bunching peak, a signature of quantum emission in CL. Fitting to a single-exponential decay model gives a lifetime of several nanoseconds, similar to lifetimes observed from SPE in other defects in h-BN.

component. Fitting reveals a series of peaks decreasing in intensity and increasing in width with increasing wavelength. The spectrum is dominated by a sharp, well-defined zero-phonon line (ZPL), centered at 436 nm (2.84 eV), with a FWHM of 10 nm (65 meV), contributing a spectral weight of ~26%, followed by several phonon replicas at 443, 461, and 484 nm (2.80, 2.69, and 2.56 eV). There is also a small, broad background component centered at 482 nm (2.57 eV). In contrast to the UV emission described above (where the phonon replicas have higher intensity than the ZPL), the relatively high intensity of the ZPL compared to the phonon replicas suggests that this emitter's coupling to the lattice is significantly weaker, a desirable quality for possible applications in future quantum information technologies. The density of emitters in Fig. 3(c) is higher than in the BP image in Fig. 2(d) and is related to the higher electron dose required for hyperspectral imaging, which will be discussed later.

Spectral information from the hyperspectral imaging can be used to perform time correlation measurements of light from the blue emitters. A bandpass filter is selected that covers a large portion of the emission peak from Fig. 3(d) in order to measure the second-order autocorrelation function using HBT intensity interferometry. Figure 3(h) shows the result of this measurement from an ensemble of emitters (see the Supplemental Material for experimental details [27]).

The majority of previous studies of light emission in h-BN have measured $g^{(2)}_{PL}(\tau)$ using PL. In stark contrast, $g^{(2)}_{CL}(\tau)$, measured in this study, exhibits a bunching peak as opposed to an antibunching dip. This behavior, which was explored previously [32,33], is attributed to simultaneous excitation of multiple color centers by the electron beam. In PL studies of defects in wide-band-gap semiconductors, such as SPEs in h-BN and NV centers in diamond, the excitation energy is typically less than the band gap of the material, resulting in the production of a single e-h pair per photon. In CL, the excitation energy is much higher than the band gap of the material, resulting in the excitation of many e-h pairs. A semiempirical relation predicts that approximately $N_{e-h} = \frac{E_0}{3E_g}$ e-h pairs are excited per incident electron [34], where E_0 is the beam energy and E_g is the band gap of h-BN. For $E_g = 6$ eV and $E_0 = 3$ keV, $N_{e-h} = 111$.

Previous work [35] showed that if the bunching peak of the $g^{(2)}_{CL}(\tau)$ function can be attributed to simultaneous excitation of an ensemble of emitters, the lifetime of the defect state can be extracted similar to an analogous PL measurement of the lifetime from the antibunching dip. An exponential fit to the time correlation data using $g^{(2)}(\tau) = 1 + a\exp(-|\tau|/\tau_{lifetime})$, with a and $\tau_{lifetime}$ being free parameters, gives a lifetime of $\tau_{lifetime} = 2.6$ ns and $g^{(2)}(0) = 1.27$. This lifetime is close in value to previous measurements of SPEs in h-BN [10–14,35]. The $g^{(2)}(0)$ value is quite low, but it has been shown that at high current, the bunching effect becomes washed out, resulting in a decreased apparent value of $g^{(2)}(0)$. While the observed bunching peak and extracted fit parameters are not incontrovertible proof that our color center is a quantum emitter, the presence of this peak is consistent with the blue emitter being a potential single-photon source.

There are two striking differences between the blue emitters shown in Fig. 2(d) and those shown in Fig. 3(c) that are

associated with the higher electron dose required to acquire an SI compared to a BP image. First, the number and density of features are higher in the SI, indicating that we are creating unique emitters by electron irradiation. Second, a variation in the shape of individual emitters appears. The emitters are round and symmetric in the BP image in Fig. 2(d), while many emitters appear to have a truncated shape in the SI component in Fig. 3(c). This truncation, discussed below, is associated with a sudden activation or deactivation event while the beam is over an emitter.

To further investigate this, we acquire a 2.5-h time series of long scan time (262 s per image) BP images over a flake of h-BN. Each image corresponds to an exposed dose of 2.3×10^7 $e^-/\text{Å}^2$ per image, with a total exposed dose of 5.7×10^8 $e^-/\text{Å}^2$. Time-series data are aligned and registered using template matching and cross correlation to correct for sample drift during the experiment. Individual emitters were automatically identified in each frame of the time series using the difference of the Gaussian blob-finding algorithm; 50 × 50 pixel regions around emitters were extracted, and image feature vectors were calculated using the principal component analysis weights of each image. Finally, false positives were removed by inspection of the output of k-means clustering on the feature vectors.

Figure 4 summarizes the results of this experiment. The top row shows the first [Fig. 4(a)], middle [Fig. 4(b)], and last [Fig. 4(c)] images from the time series at full spatial resolution. The colored boxes in the full-resolution images indicate regions where we have cropped the data and displayed the entire time series in a 300-nm region around four emitters [Figs. 4(d)–4(g)]. Figure 4(d) shows an emitter that is suddenly activated by the electron beam (indicated by the truncated disk shape of the emitter), remains in the emissive state for five frames, then suddenly switches off for the remainder of the time series. Figures 4(e) and 4(f) show emitters that switch on and off several times throughout the scan. Some of these activation and deactivation events appear as truncated disks [shown in detail in Figs. 4(h) and 4(i)], while some appear as the sudden appearance or disappearance of a bright spot from one frame to another. Figure 4 illustrates that not only are the emitters activated and deactivated by the electron beam, but they also disappear and reappear in identical spatial locations (within the accuracy of our measurement).

We note that we have also attempted characterization of these emitters using PL. NIMS-BN samples on indexed Si substrates are seeded with emitters using the SEM, characterized using CL, and then transferred to a cw PL setup using 1-mW, 349-nm; 10-mW, 405-nm; and 30-mW, 532-nm excitation focused to a diffraction-limited spot. No emission is observed in the UV-Vis range using the available excitation energies and intensities within reasonable integration times. This fact, in conjunction with the activation-deactivation behavior observed under the electron beam, hints that the origin of this emission is associated with the charge state of an electron-irradiated point defect, similar to SPEs in other semiconductor systems [36–38].

Furthermore, we note that the blue 435-nm emission is not observed using PL or CL in any samples of commercial h-BN
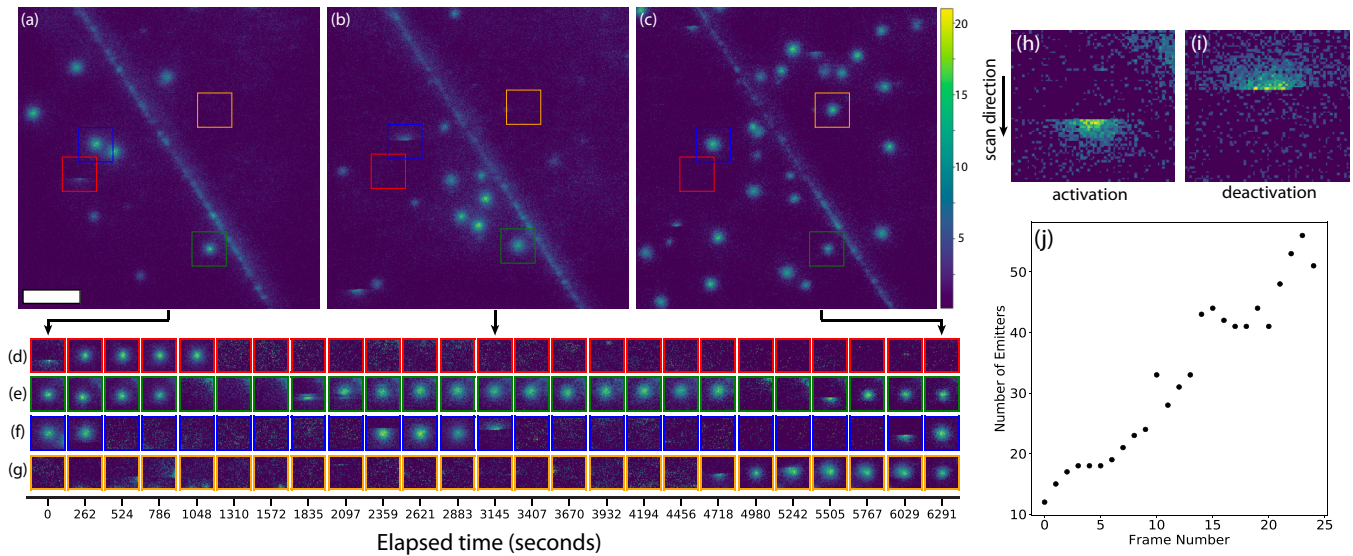
FIG. 4. Overview of switching behavior in h-BN emitters. A series of CL bandpass images (409- -482 nm) are taken over 1.5 h at 4.5 min per image, with each time point corresponding to a single image scan with an electron beam dose of $2.3 \times 10^7 \ e^-/\text{Å}^2$. The top row shows the first, middle, and final images in the series at full spatial resolution (scale bar is 500 nm, color scale is in units of counts/pixel). The bottom row shows the dynamic behavior of four separate 300-nm regions (indicated by the colored boxes in the top panel) over the entire time series. The emitters exhibit clear switching behavior, turning on and off between frames of the time series. Examples of emitters that suddenly turn on or off as the beam is passing over are shown in (h) and (i), respectively. (j) shows that the number of emitters in each frame grows roughly linearly with electron beam dose.

powder. This implies that this emission may be closely related to the unique synthetic origin of NIMS-BN.

IV. DISCUSSION

We consider possible mechanisms for our emission. We immediately rule out the direct creation of defects via knock-on damage and electron-beam-induced heating. The electron energy threshold for knock-on damage in h-BN is in the range of 70–80 keV [39,40], far greater than the 1–10 keV energy range of the SEM beam. Electron-beam-induced heating is unlikely due to the high thermal conductivity of h-BN along with the relatively low current of the electron beam.

The change in temperature of the sample can be estimated [41] assuming that energy from the electron beam is uniformly deposited in a sphere of radius R using $\Delta T = 3IVf/2\pi R\kappa$, where I is the beam current, V is the beam accelerating voltage, f is the fraction of incident energy that is absorbed, and κ is the thermal conductivity of h-BN (600 W/m K). Assuming that 100% of the incoming power is absorbed in a spherical interaction volume of radius $R = 30$ nm, a 2-keV electron beam with 1 nA of current causes a temperature increase of $\Delta T = 0.05$ K. This value would be even lower at increased accelerating voltage [42] because the interaction size scales approximately as $V^{1.75}$. Furthermore, due to the finite thickness of an h-BN flake, the fraction of energy from the beam deposited into the sample decreases at higher beam energies.

We propose that the origin of this unique emitter is electron-beam-induced defect chemistry, outlined in Fig. 5. The as-synthesized NIMS-BN crystal has some initial concentration of vacancies and intercalated interstitials, illustrated in

the cartoon in Fig. 5(a). Electron-beam-induced diffusion increases the mobility of the interstitials, causing the impurities to diffuse towards the naturally occurring vacancies within the material, resulting in the interstitial and vacancy combining into a defect complex [43,44] [Fig. 5(b)]. We propose that the activation-deactivation behavior results from electron-beam-induced charge state switching of the color centers, similar to previous observations of NV centers in diamond [45]. In our model, the electron beam modifies the charge state of the defect, causing it to change from a nonemissive to an emissive state, resulting in the production of photons [Fig. 5(c)]. The charge state of the defect can also be modified in the opposite sense, resulting in emitters switching on and off during a mea-
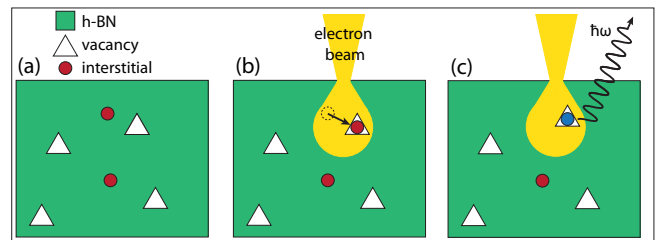

FIG. 5. Proposed model for formation and activation of blue color centers in NIMS-BN. The as-synthesized material has some intrinsic density of interstitial impurities and lattice vacancies, as shown in (a). When stimulated by the electron beam, the impurity atoms are driven into the vacancies, and due to the energy provided by the beam a substitutional defect complex is formed. The charge state of the defect is changed by the beam causing it to emit photons. The charge state of the defect is sensitive to the intense stimulus from the electron probe and can jump between emissive and nonemissive states, resulting in a blinking effect.

surement. We do not see any evidence of emitters switching or blinking to a different emission band in our experiments. This effect would be fairly obvious in the SIs and would appear as a distinct component, complementary to the one shown in Figs. 3(c) and 3(d). The spatial loading would appear as a collection of pointlike emitters accompanied by a set of truncated disks [truncated in the opposite sense of those in Fig. 3(c)].

This change in charge state has two possible origins. One scenario is that incident beam and secondary electrons are captured by the defect complex, resulting in a negative charge state. Alternatively, the incident or secondary electrons ionize the defect, resulting in a positive charge state. Currently, neither possibility can be excluded, suggesting future experiments and calculations. Previous studies have shown that a low-energy electron beam can cause diffusion of impurities or vacancies, vacancy-impurity defect reconstruction, and charge state switching in other wide-band-gap semiconductors. While speculative, our proposed model is consistent with previous findings of electron-beam-induced luminescent diamond NV centers [46].

We propose that this emission has not been previously observed in h-BN for several reasons. Past studies of color centers in h-BN have typically not used NIMS-BN, which has a unique synthetic origin, but rather commercially obtained h-BN. We surmise that the Ba-B-N solvent precursor used in the NIMS-BN synthesis could produce barium impurities in these samples, which would not be present in commercially obtained material synthesized using different growth precursors. Under the assumptions of our model, this emission would not be observed in the absence of this unique impurity. PL studies of color centers in h-BN that do use NIMS-BN have used a 532-nm laser excitation to probe the sample and have focused on light emission in a high-wavelength range. This excitation energy is too low to probe a state that emits at 435 nm. It is likely that the charge recombination dynamics in this regime are dominated by nonradiative transitions. It is possible that the 435-nm emission is only present using CL because of the large number of electron-hole pairs created per incident electron, as well as the high intensity of the electron probe. A final, more speculative reason that this emission has not been observed to date is the possibility that the particular defect complex responsible for the emission needs the high-energy density of the electron beam in order to drive interstitial-vacancy recombination.

Our experimental results of the spectral and spatial character of this emitter in h-BN show many features observed in quantum emitters, suggesting that this unique color center is a potential source of single photons. The emission is highly localized and spectrally pure, exhibits a ZPL with phonon replicas, and can be modified with an electron beam, all features of SPEs in other solid-state systems. The bunching behavior seen in the $g^{(2)}(\tau)$ measurement, while not proof of single-photon emission, is not inconsistent with electron-beam-induced light emission from an ensemble of quantum emitters. While all observations are *consistent with* the behavior of a two-level-like system capable of single-photon emission, further study is required to unambiguously confirm the quantum nature of this emitter.

V. CONCLUSION

We have identified a color center unique to high-quality hexagonal boron nitride using cathodoluminescence in the SEM. The emission is peaked at 435 nm and has spectral characteristics indicative of weak lattice coupling. The electron beam activates and deactivates emission from point defects in the crystal. We have proposed that this emission originates from a barium atom interstitial impurity forming a defect complex with a vacancy driven by the energy of the electron beam. The charge state of this defect is changed by the electron beam resulting in the emitters switching on and off.

ACKNOWLEDGMENTS

[1] H.-K. Lo, M. Curty, and K. Tamaki, Secure quantum key distribution, Nat. Photonics **8**, 595 (2014).

[2] V. Scarani, H. Bechmann-Pasquinucci, N. J. Cerf, M. Dusek, N. Lutkenhaus, and M. Peev, The security of practical quantum key distribution, Rev. Mod. Phys. **81**, 1301 (2009).

[3] P. Kok, W. J. Munro, K. Nemoto, T. C. Ralph, J. P. Dowling, and G. J. Milburn, Linear optical quantum computing with photonic qubits, Rev. Mod. Phys. **79**, 135 (2007).

[4] J. L. O'Brien, A. Furusawa, and J. Vučković, Photonic quantum technologies, Nat. Photonics **3**, 687 (2009).

[5] T. E. Northup and R. Blatt, Quantum information transfer using photons, Nat. Photonics **8**, 356 (2014).

[6] C. Kurtsiefer, S. Mayer, P. Zarda, and H. Weinfurter, Stable Solid-State Source of Single Photons, Phys. Rev. Lett. **85**, 290 (2000).

[7] P. Neumann, N. Mizuochi, F. Rempp, P. Hemmer, H. Watanabe, S. Yamasaki, V. Jacques, T. Gaebel, F. Jelezko, and J. Wrachtrup, Multipartite entanglement among single spins in diamond, Science **320**, 1326 (2008).

[8] S. Castelletto, B. C. Johnson, V. Ivády, N. Stavrias, T. Umeda, A. Gali, and T. Ohshima, A silicon carbide room-temperature single-photon source, Nat. Mater. **13**, 151 (2014).

[9] A. J. Morfa, B. C. Gibson, M. Karg, T. J. Karle, A. D. Greentree, P. Mulvaney, and S. Tomljenovic-Hanic, Single-photon emission and quantum characterization of zinc oxide defects, Nano Lett. **12**, 949 (2012).

[10] L. J. Martinez, T. Pelini, V. Waselowski, J. R. Maze, B. Gil, G. Cassabois, and V. Jacques, Efficient single photon emission from a high-purity hexagonal boron nitride crystal, Phys. Rev. B **94**, 121405(R) (2016).

[11] T. T. Tran, C. Zachreson, A. M. Berhane, K. Bray, R. G. Sandstrom, L. H. Li, T. Taniguchi, K. Watanabe, I. Aharonovich, and M. Toth, Quantum Emission from Defects in Single-Crystalline Hexagonal Boron Nitride, Phys. Rev. Appl. **5**, 034005 (2016).

[12] T. T. Tran, C. Elbadawi, D. Totonjian, C. J. Lobo, G. Grosso, H. Moon, D. R. Englund, M. J. Ford, I. Aharonovich, and M. Toth, Robust multicolor single photon emission from point defects in hexagonal boron nitride, ACS Nano **10**, 7331 (2016).

[13] T. T. Tran, K. Bray, M. J. Ford, M. Toth, and I. Aharonovich, Quantum emission from hexagonal boron nitride monolayers, Nat. Nanotechnol. **11**, 37 (2016).

[14] R. Bourrellier, S. Meuret, A. Tararan, O. Stéphan, M. Kociak, L. H. G. Tizei, and A. Zobelli, Bright UV single photon emission at point defects in h-BN, Nano Lett. **16**, 4317 (2016).

[15] N. G. Chopra, R. J. Luyken, K. Cherrey, V. H. Crespi, M. L. Cohen, S. G. Louie, and A. Zettl, Boron nitride nanotubes, Science **269**, 966 (1995).

[16] A. Rubio, J. L. Corkill, and M. L. Cohen, Theory of graphitic boron nitride nanotubes, Phys. Rev. B **49**, 5081 (1994).

[17] K. S. Novoselov, D. Jiang, F. Schedin, T. J. Booth, V. V. Khotkevich, S. V. Morozov, and A. K. Geim, Two-dimensional atomic crystals, Proc. Natl. Acad. Sci. U.S.A. **102**, 10451 (2005).

[18] A. Nagashima, N. Tejima, Y. Gamou, T. Kawai, and C. Oshima, Electronic dispersion relations of monolayer hexagonal boron nitride formed on the Ni(111) surface, Phys. Rev. B **51**, 4606 (1995).

[19] D. Golberg, Y. Bando, O. Stéphan, and K. Kurashima, Octahedral boron nitride fullerenes formed by electron beam irradiation, Appl. Phys. Lett. **73**, 2441 (1998).

[20] C. R. Dean, A. F. Young, I. Meric, C. Lee, L. Wang, S. Sorgenfrei, K. Watanabe, T. Taniguchi, P. Kim, K. L. Shepard, and J. Hone, Boron nitride substrates for high-quality graphene electronics, Nat. Nanotechnol. **5**, 722 (2010).

[21] T. Pham, A. L. Gibb, Z. Li, S. M. Gilbert, C. Song, S. G. Louie, and A. Zettl, Formation and dynamics of electron-irradiation-induced defects in hexagonal boron nitride at elevated temperatures, Nano Lett. **16**, 7142 (2016).

[22] S. M. Gilbert, G. Dunn, A. Azizi, T. Pham, B. Shevitski, E. Dimitrov, S. Liu, S. Aloni, and A. Zettl, Fabrication of subnanometer-precision nanopores in hexagonal boron nitride, Sci. Rep. **7**, 15096 (2017).

[23] S. M. Gilbert, T. Pham, M. Dogan, S. Oh, B. Shevitski, G. Schumm, S. Liu, P. Ercius, S. Aloni, M. L. Cohen, and A. Zettl, Alternative stacking sequences in hexagonal boron nitride, 2D Mater. **6**, 021006 (2019).

[24] T. Taniguchi and K. Watanabe, Synthesis of high-purity boron nitride single crystals under high pressure by using Ba-BN solvent, J. Cryst. Growth **303**, 525 (2007).

[25] D. B. Durham, D. F. Ogletree, and E. S. Barnard, Scanning Auger spectromicroscopy using the ScopeFoundry software platform, Surf. Interface Anal. **50**, 1174 (2018).

[26] R. Brouri, A. Beveratos, J.-P. Poizat, and P. Grangier, Photon antibunching in the fluorescence of individual color centers in diamond, Opt. Lett. **25**, 1294 (2000).

[27] See Supplemental Material at http://link.aps.org/supplemental/10.1103/PhysRevB.100.155419 for a description of $g^{(2)}$ measurement, detailed results of peak fitting to the blue color center emission spectrum, and detailed results of multivariate statistical analysis of hyperspectral imaging data.

[28] F. de la Peña, T. Ostasevicius, V. Tonaas Fauske, P. Burdet, E. Prestat, P. Jokubauskas, M. Nord, M. Sarahan, K. E. MacArthur, D. N. Johnstone, J. Taillon, J. Caron, V. Migunov, T. Furnival, A. Eljarrat, S. Mazzucco, T. Aarholt, M. Walls, T. Slater, F. Winkler, B. Martineau, G. Donval, R. McLeod, E. R. Hoglund, I. Alxneit, I. Hjorth, T. Henninen, L. Fernando Zagonel, A. Garmannslund, and 5ht2, HYPERSPY/HYPERSPY v1.5.2, https://zenodo.org/record/3396791 (2019).

[29] P. Jaffrennou, J. Barjon, J.-S. Lauret, B. Attal-Trétout, F. Ducastelle, and A. Loiseau, Origin of the excitonic recombinations in hexagonal boron nitride by spatially resolved cathodoluminescence spectroscopy, J. Appl. Phys. **102**, 116102 (2007).

[30] N. V. Proscia, Z. Shotan, H. Jayakumar, P. Reddy, C. Cohen, M. Dollar, A. Alkauskas, M. Doherty, C. A. Meriles, and V. M. Menon, Near-deterministic activation of room-temperature quantum emitters in hexagonal boron nitride, Optica **5**, 1128 (2018).

[31] M. Arngren, M. N. Schmidt, and J. Larsen, Unmixing of hyperspectral images using bayesian non-negative matrix factorization with volume prior, J. Signal Process. Syst. **65**, 479 (2011).

[32] M. A. Feldman, E. F. Dumitrescu, D. Bridges, M. F. Chisholm, R. B. Davidson, P. G. Evans, J. A. Hachtel, A. Hu, R. C. Pooser, R. F. Haglund, and B. J. Lawrie, Colossal photon bunching in quasiparticle-mediated nanodiamond cathodoluminescence, Phys. Rev. B **97**, 081404(R) (2018).

[33] S. Meuret, T. Coenen, H. Zeijlemaker, M. Latzel, S. Christiansen, S. Conesa-Boj, and A. Polman, Photon bunching reveals single-electron cathodoluminescence excitation efficiency in InGaN quantum wells, Phys. Rev. B **96**, 035308 (2017).

[34] C. A. Klein, Bandgap dependence and related features of radiation ionization energies in semiconductors, J. Appl. Phys. **39**, 2029 (1968).

[35] S. Meuret, L. H. G. Tizei, T. Cazimajou, R. Bourrellier, H. C. Chang, F. Treussart, and M. Kociak, Photon Bunching in Cathodoluminescence, Phys. Rev. Lett. **114**, 197401 (2015).

[36] M. V. Hauf, B. Grotz, B. Naydenov, M. Dankerl, S. Pezzagna, J. Meijer, F. Jelezko, J. Wrachtrup, M. Stutzmann, F. Reinhard, and J. A. Garrido, Chemical control of the charge state of nitrogen-vacancy centers in diamond, Phys. Rev. B **83**, 081304(R) (2011).

[37] P. Siyushev, H. Pinto, M. Voros, A. Gali, F. Jelezko, and J. Wrachtrup, Optically Controlled Switching of the Charge State

of a Single Nitrogen-Vacancy Center in Diamond at Cryogenic Temperatures, Phys. Rev. Lett. **110**, 167402 (2013).

[38] B. Grotz, M. V. Hauf, M. Dankerl, B. Naydenov, S. Pezzagna, J. Meijer, F. Jelezko, J. Wrachtrup, M. Stutzmann, F. Reinhard, and J. A. Garrido, Charge state manipulation of qubits in diamond, Nat. Commun. **3**, 729 (2012).

[39] J. Kotakoski, C. H. Jin, O. Lehtinen, K. Suenaga, and A. V. Krasheninnikov, Electron knock-on damage in hexagonal boron nitride monolayers, Phys. Rev. B **82**, 113404 (2010).

[40] A. Zobelli, A. Gloter, C. P. Ewels, G. Seifert, and C. Colliex, Electron knock-on cross section of carbon and boron nitride nanotubes, Phys. Rev. B **75**, 245402 (2007).

[41] L. Reimer, *Scanning Electron Microscopy: Physics of Image Formation and Microanalysis*, 2nd ed., Vol. 45 (Springer, Berlin, Heidelberg, 2013).

[42] C. Donolato, An analytical model of SEM and STEM charge collection images of dislocations in thin semiconductor layers.

II. EBIC images of dislocations, Phys. Status Solidi A **66**, 445 (1981).

[43] O. Dyck, S. Kim, S. V. Kalinin, and S. Jesse, Placing single atoms in graphene with a scanning transmission electron microscope, Appl. Phys. Lett. **111**, 113104 (2017).

[44] B. M. Hudak, J. Song, H. Sims, M. C. Troparevsky, T. S. Humble, S. T. Pantelides, P. C. Snijders, and A. R. Lupini, Directed atom-by-atom assembly of dopants in silicon, ACS Nano **12**, 5873 (2018).

[45] T. Gaebel, M. Domhan, C. Wittmann, I. Popa, F. Jelezko, J. Rabeau, A. Greentree, S. Prawer, E. Trajkov, P. Hemmer, and J. Wrachtrup, Photochromism in single nitrogen-vacancy defect in diamond, Appl. Phys. B **82**, 243 (2006).

[46] J. Schwartz, S. Aloni, D. F. Ogletree, and T. Schenkel, Effects of low-energy electron irradiation on formation of nitrogen-vacancy centers in single-crystal diamond, New J. Phys. **14**, 043024 (2012).